Energy & Environmental Science

Cite this: *Energy Environ. Sci.*, 2011, **4**, 4410

www.rsc.org/ees

PERSPECTIVE

Organic solar cells: A new look at traditional models

Jonathan D. Servaites,[ab] Mark A. Ratner*[abc] and Tobin J. Marks*[abc]

Received 8th May 2011, Accepted 13th July 2011
DOI: 10.1039/c1ee01663f

Traditional inorganic solar cell models, originating with the work of Shockley, are widely used in understanding bulk heterojunction (BHJ) organic solar cell response (organic solar cells are also referred to as organic photovoltaics, or OPVs). While these models can be useful, there are several key points of departure from traditional solar cell behavior. In this Perspective, we discuss three important areas: (1) geminate pair and bimolecular recombination, (2) effects of interfacial layers inserted between the electrodes and active layer, and (3) resistance effects. Since organic solar cell materials typically have large Coulombic exciton binding energies (*e.g.*, ~0.3–0.5 eV), limited dissociation of photogenerated charge carriers can be a significant limitation in these cells that is not observed in traditional silicon solar cells. Additionally, the active layer morphology of BHJ organic solar cells allows free charge carriers to recombine before extraction from the cell, creating another photocurrent loss mechanism. Interfacial layers serve a unique role in BHJ organic solar cells; in addition to conventional functions such as photon transmission and charge injection, interfacial layers often act as "blocking" layers, ensuring that charge carriers are collected at their respective electrodes (*i.e.*, electrons at the cathode and holes at the anode). Additionally, resistance effects in organic solar cells differ from traditional models in both field and cell area dependencies. Organic semiconductor mobilities and charge densities exhibit significant sensitivity to field strength, with mobility varying by ~10x over typical cell voltage test ranges (1 V). This creates the need for alternative models to describe cell internal resistance. Finally, resistance losses are also sensitive to cell area, due to the limited conductivities of the transparent electrode materials used. Therefore, accommodation of the above deviations from traditional models is imperative for the design and synthesis of new generation high efficiency organic solar cell materials.

[a]*Department of Materials Science and Engineering, Northwestern University, 2145 Sheridan Road, Evanston, IL, 60208-3113, USA. E-mail: ratner@chem.northwestern.edu; t-marks@northwestern.edu*
[b]*Department of Chemistry, Northwestern University, 2145 Sheridan Road, Evanston, IL, 60208-3113, USA*
[c]*Argonne-Northwestern Solar Energy Research Center (ANSER), Northwestern University, 2145 Sheridan Road, Evanston, IL, 60208-3113, USA*

1. Introduction

Organic photovoltaic (OPV) cells[1–19] offer the potential to change the landscape of how we produce and use energy. If developed into a mature technology, they offer the opportunity to significantly reduce solar energy costs by employing earth-abundant materials, efficient installation, and roll-to-roll production.[4–6]

Broader context

The development of new energy technologies is crucial for climate stability and global security. Meanwhile, solar energy resources are vast: more energy reaches our planet in one hour than humankind consumes in an entire year. However, solar technologies have thus far only been used to a limited degree in energy production because of high costs. Organic solar cells offer a potential route to large-scale solar deployment based on the possibility of large cost reductions using earth-abundant materials and inexpensive production technologies. Nevertheless, despite recent advances in performance, organic solar cell efficiencies lag behind their inorganic counterparts, and new materials are needed to enhance performance. Furthermore, existing performance limitations are not completely understood and are a reason for organic solar cells not yet reaching their full potential. In this Perspective, we consider key areas in which organic solar cell function differs from traditional models. Designing materials through effective new models will help this promising new solar technology achieve high performance levels and enable solar technologies to achieve large-scale energy production.

Their properties and designs can be tuned and optimized based on materials versatility, solution-based processing, and mechanical flexibility.[4,6–8] In recent years, there have been steady improvements in OPV power conversion efficiencies, with the 8% threshold recently crossed.[2,20–24] Note that, according to media reports, efficiencies as high as 9.2% have been achieved; the highest confirmed OPV efficiency to date is ~8.3%.[23,24] While these efficiencies are significantly less than today's commercial inorganic solar cells, the steady improvement in efficiencies has generated significant interest in the potential for OPVs to offer practical, widespread energy production. In addition to durability requirements, increasing the OPV power conversion efficiencies (PCE) to >10% is regarded as an important threshold for widespread deployment. For efficiencies <10%, the cost of installation is typically too expensive for widespread energy production, even if the solar cells and modules are inexpensive.[25,26] (However, niche applications are relevant for low PCE solar cells when other benefits such as flexibility or portability are offered.) Therefore, to achieve these efficiency advances, major materials and cell design advances are needed, and we believe that achieving these developments will require better understanding of organic solar cell loss mechanisms before high efficiencies can be achieved. There exist crucial differences between organic and traditional inorganic *p-n* junction[27–34] solar cells; this article identifies and analyzes what we regard as key areas of differentiation between these solar cell classes and suggests some ways in which OPV efficiencies can be significantly improved.

Fig. 1 presents an illustration of a bulk heterojunction (BHJ)[12] OPV cell. The typical structure, from top to bottom, consists of a transparent electrode, which is generally composed of glass coated with a transparent conducting oxide, usually tin-doped indium oxide (ITO). This is followed by an interfacial layer (typically an organic or metal oxide layer). Next, the absorber (active) layer, which is responsible for the photovoltaic activity of the cell, consists of an interpenetrating network of electron donor (hole-transporting) and acceptor (electron-transporting) materials. In state-of-the-art systems, the donor is generally the light-absorbing material; however, recent research has also focused on light-absorbing acceptors.[26,35] Finally, the bottom contact typically consists of a second interfacial layer (*e.g.*, LiF or TiO_x)[11,26] and a low work function metal electrode, such as aluminum.

Unlike the case in polycrystalline silicon solar cells, the electron-hole binding energy in organic solar cells is high (*e.g.*, ~0.3–0.5 eV)[26,36,37] so that light absorption leads to the generation of a bound electron-hole pair known as an exciton; ref. 36, 37, and 38 provide useful background information on exciton binding energies. To split the exciton and create electrical current, an energetic offset at the donor–acceptor interface can be employed to overcome this binding energy. Excitons diffuse from their photogeneration point until reaching one of these interfaces (Fig. 1). In the case where the donor material is the primary light absorber, the photoexcited electron from this bound pair is then transferred to the acceptor, forming a charge transfer state at the interface with the electron on the acceptor and hole on the

Jonathan D. Servaites

Jonathan Servaites began a postdoctoral position at Stanford University in June 2011, where he is developing atomic layer deposition (ALD) for nanoscale photovoltaics. He completed his Ph.D. in May 2011 at Northwestern University (MSE), where he researched designs for high efficiency organic photovoltaic (OPV) cells and founded a solar technology company. Prior to his Ph.D. studies, Dr. Servaites worked at two energy technology start-ups and received a B.S. from Stanford in Chemical Engineering and an M.S. from UC Berkeley in Energy & Resources.

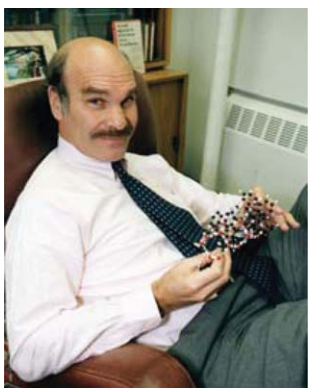

Mark A. Ratner

Mark Ratner is the Dumas University Professor at Northwestern University. He is interested in nanoscale structure and function, along with theory of fundamental chemical processes. He tries to bring together structure and function in molecular nanostructures, based on theoretical notions, on exemplary calculations, and (very importantly) on collaborations with experimentalists and other theorists. Areas of interest include molecular electronics, electron transfer, self-assembly, nanoscience and technology, energy systems and processes, and theories of quantum dynamics. Dr. Ratner received a B.S. from Harvard University and a Ph.D. from Northwestern University in Chemistry.

Tobin J. Marks

Tobin Marks is the V. N. Ipatieff Professor of Chemistry at Northwestern University. He received the 2006 U.S. National Medal of Science, the 2008 Principe de Asturias Prize, the 2009 the MRS Von Hippel Award, and the 2011 Dreyfus Prize. His research interests include organo-f-element and transition metal organometallic chemistry, oxide materials chemistry, catalysis, and organic opto-electronic materials. He is a member of the U.S., German, and Indian National Academies of Sciences, a Fellow of the Royal Society of Chemistry, and of the American Academy of Arts and Sciences. Dr. Marks received a B.S. from the University of Maryland and a Ph.D. from MIT in Chemistry.

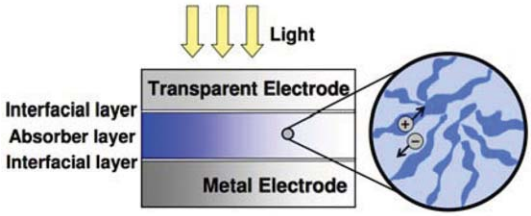

Fig. 1 Diagram of a bulk heterojunction organic solar cell.

donor.[26,39–46] The dissociation-recombination dynamics of this "geminate pair" state are of critical importance in achieving high efficiency organic solar cells and are discussed in greater detail in Section 3. Furthermore, the architecture of the BHJ OPV cell is unique due to two competing length scales: exciton diffusion distances are on the order of 10 nm[47] before exciton decay, whereas typical active layer thicknesses required for optimum light absorption are >100 nm.[26] In order to (1) position donor–acceptor interface sites within ~10 nm of the photon absorption site *while* (2) absorbing the majority of light with energies above the donor bandgap, the BHJ OPV architecture of placing donor–acceptor interfaces throughout the active layer bulk has been extensively explored and refined.[26] This design has afforded impressive internal quantum efficiencies approaching 100% for photons with energies greater than the absorber bandgap.[10] Note that we define internal quantum efficiency here as the probability that a photon absorbed by the active layer is converted into collected charge at the electrodes at cell voltage = 0.

Finally, the influence of BHJ OPV active layer morphology on materials and device characteristics, including mobility, internal resistance, and recombination rates, has been highlighted in numerous studies. For example, studies have correlated processing conditions with morphology changes and resulting charge carrier mobilities.[35,48] Likewise, recent reports have evaluated the importance of active layer nanostructure on recombination rates[49–51] (both "geminate pair" and "bimolecular" – see Section 3 for further details on these recombination mechanisms). While OPV nanomorphology is not the focus of this Perspective article, numerous reviews and reports provide useful information on this crucial OPV topic.[6,19,35,42,50,52–55]

There are therefore dramatic differences between organic solar cells and traditional silicon cells in terms of materials properties (*e.g.*, light absorption profiles, carrier binding energies, and mobilities) and device design (*e.g.*, absorber layer architecture, and active layer thickness). Despite these differences, traditional performance models originally based upon Shockley's *p-n* junction model[30] have been transferred from silicon cells and applied to their BHJ organic counterparts.[8,56–60] This traditional model can be a useful tool in understanding organic solar cell limitations; however, there exist key areas where the model must be modified to appropriately account for the distinctive characteristics of BHJ OPV response. With this objective in mind, we address here three key areas relating to OPV function and efficiency: (1) recombination mechanisms, (2) interfacial layers, and (3) field- and cell area-dependent resistance. There are additional important points of differentiation beyond these areas, however we believe these three provide a foundation for understanding how organic solar cell behavior diverges from traditional models. Note that there are several reports on alternative descriptions of current–voltage behavior in OPVs that provide useful physical insight into these systems; for example, see ref. 61, 62, 63, and 64. We begin our analysis in Section 2 by first outlining the fundamentals of the traditional inorganic model. In Section 3, we examine two recombination mechanisms that are unaccounted for in the traditional model – bimolecular and geminate pair recombination. In Section 4, we address the unique role of interfacial layers for BHJ OPVs in providing selective contacts or filters at the electrodes, ensuring that primarily (or exclusively) electrons are collected at one electrode and holes at the other. Finally, in Section 5, we evaluate the importance of field-dependent resistance and cell area.

2. Fundamentals of the traditional solar cell model

The traditional inorganic solar cell model is a relatively simple and useful tool for describing cell response, bottlenecks, and areas for efficiency enhancement. Nevertheless, the unique physical and electrical complexities of organic solar cells require a thorough understanding of the assumptions of the traditional model, where they apply, and what modifications are required to account for OPV behavior. We begin by introducing the basics of the traditional model. Fig. 2 below provides current density-voltage (*JV*) curves typical of organic solar cells. The blue curves in Fig. 2a and 2b are from identical data sets – only that Fig. 2a is on a linear scale and Fig. 2b is on a semilog scale; these data are the so-called "dark data" (*i.e.*, the *JV* response of the cell in the dark).[65] The black curve in Fig. 2a is based on the illuminated (or light) data, accounting for the *JV* response under solar illumination. The photogenerated current is treated as independent of cell voltage, as shown in the J_{ph} curve in Fig. 2a; in the next section, we will examine ways in which this assumption does not hold for OPVs. Traditional theory applies the superposition principle in comparing the dark and illuminated data; after correcting for resistance losses, superimposing the constant photocurrent (J_{ph}) and dark *JV* data produces the illuminated *JV* curve.[58,65] Regions I, II, and III are explained below.

Fig. 3 depicts the widely used equivalent circuit solar cell model. It deconstructs the solar cell *JV* behavior into four constituent parts: a photocurrent source, diode, series resistor, and shunt resistor. The photocurrent source is simply the result of converting absorbed photons to free charge by the solar cell, the diode represents electron-hole recombination at the *p-n* junction, the series resistor accounts for the internal resistance of the cell to current flow, and the shunt resistor models leakage current through the cells (*e.g.*, *via* pinholes). Mathematically this model is represented by the relationship:

$$J = \underbrace{J_0\left[\exp\left(\frac{e(V - JR_s)}{nk_BT}\right) - 1\right]}_{\text{Recombination current}} + \underbrace{\frac{V - JR_s}{R_{sh}}}_{\text{Shunt current}} - \underbrace{J_{ph}}_{\text{Photocurrent}}, \quad (1)$$

where J_0 is the reverse bias saturation current density, e is the elementary charge, R_s is the series resistance, n is the diode ideality factor, k_B is Boltzmann's constant, T is temperature, and R_{sh} is the shunt resistance. According to the original *p-n* junction theory of Shockley, J_0 represents the saturation current density at reverse bias for an *ideal p-n* junction diode.[30] For this ideal

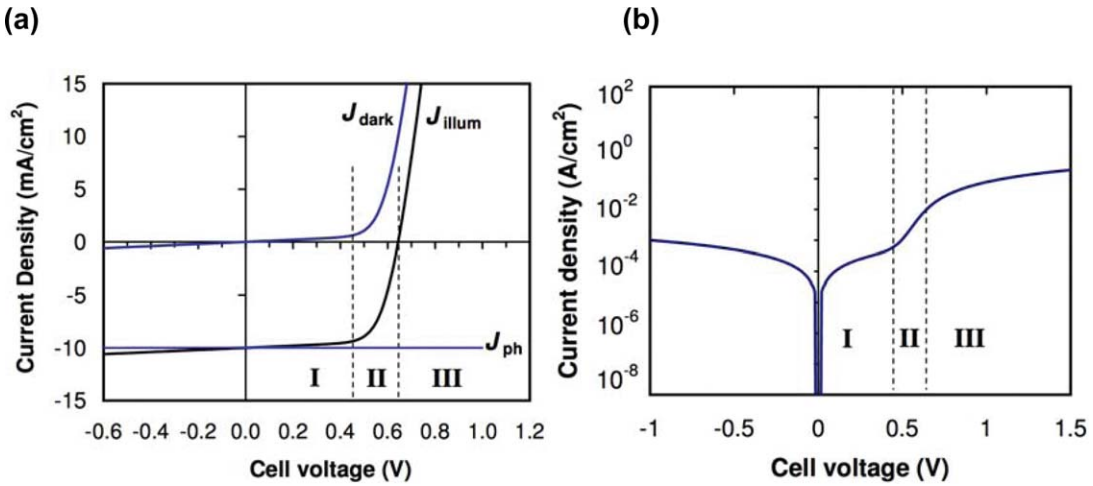

Fig. 2 (a) Typical dark *JV* plot (semilog scale) for an organic solar cell. The three regions indicated account for where different effects dominate: Region I accounts for leakage (shunt) currents, Region II recombination currents, and Region III series resistance. (b) This *JV* curve is from identical data as the blue (J_{dark}) curve in part (a), only presented on a semilog plot and using the absolute value of current density (negative current densities cannot be plotted on a log scale). Note that at $V = 0$, the dark current density = 0.

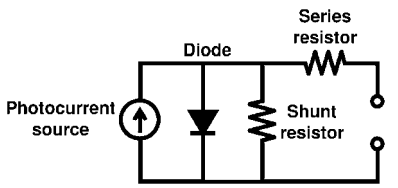

Fig. 3 The traditional equivalent circuit model for solar cells.[32] Important deviations from this model must be addressed in understanding organic solar cell behavior. Note that the diode represents recombination current.

diode, $n = 1$. Later, accounting for Shockley-Read-Hall recombination due to defect states at the *p-n* junction, models were developed for n > 1.[29,31] The "recombination current" portion of eqn (1) therefore accounts for how a solar cell acts as a diode in the dark. The shunt current in eqn (1) represents cell leakages, due to sources such as pinholes that enable parasitic current to move directly from one electrode to the other. As $R_{sh} \rightarrow \infty$, the shunt current approaches zero (which is desirable, since it is a parasitic current). In optimized solar cells – including OPVs – the shunt current is often negligible.[48] In Figs. 2a and 2b, Regions I, II, and III illustrate how the different components of the solar cell equivalent circuit (Fig. 3) dominate the *JV* response of the cell at different voltages. At low voltages (Region I), the *JV* characteristics are primarily determined by R_{sh}, at intermediate voltages (Region II) by the diode parameters J_0 and n, and at high voltages (Region III) by R_s. These regions provide useful rules of thumb when evaluating a *JV* response curve: for instance, a steep slope in Region III generally means a low R_s device. However, as will be developed in greater detail throughout this article, there are key aspects of organic solar cells to consider in applying this model. Finally, three commonly used solar cell figures of merit are: short circuit current density (J_{sc}), open circuit voltage (V_{oc}), and fill factor. At $V = 0$, J_{sc} is the cell current density, and at $J = 0$, V_{oc} is the cell voltage. A cell will generally be operated at an intermediate current density (J_{oper}) and voltage (V_{oper}) where power density is maximized ($P_{max} = J_{oper}V_{oper}$). The fill factor is equal to $(J_{oper}V_{oper})/(J_{sc}V_{oc})$, accounting for how "square" the *JV* curve is.[32–34]

3. New electron-hole losses at the donor–acceptor interface: geminate pair and bimolecular recombination

3.1. Geminate pair *vs.* bimolecular recombination

Two key loss mechanisms operative in OPVs are illustrated in Fig. 4: geminate pair (Fig. 4a) and bimolecular recombination (Fig. 4b) losses.[42] Fig. 4a shows that an electron-hole pair initially undergoes dissociation at the interface of donor (with positive charge) and acceptor (with negative charge) materials regions, but the pair typically remains bound at the interface due to the electron-hole Coulombic attraction – *i.e.*, the geminate pair binding energy. In order to proceed to the electrodes, the two charge carriers must therefore overcome this barrier. There are three competing processes at this moment: complete dissociation of the geminate pair (*i.e.*, overcoming the Coulombic barrier), relaxation of the initial Franck–Condon vibrational energy in the geminate pair, and recombination at this donor–acceptor interface. Furthermore, Fig. 4b illustrates bimolecular recombination: after the geminate pair has completely dissociated into free charge carriers, there exists the possibility of electrons and holes colliding and recombining, before collection at their respective electrodes.

The above two mechanisms have been widely investigated in a range of organic materials systems, including evaluation of the dominant loss mechanism *vs.* competing mechanisms.[39,41,42,66–72] We do not intend to resolve these particular issues here and, in fact believe that both mechanisms are important for organic solar cells and that the relative contributions are system-dependent. Given the wide range of materials systems and morphologies currently under investigation in OPVs, different weightings of loss contributions are expected. However, in understanding

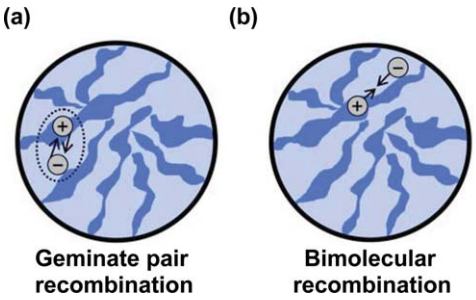

Fig. 4 Illustrations of (a) geminate pair dissociation and (b) bimolecular recombination loss mechanisms in OPVs.

organic solar cell response, it is of critical importance to understand how these losses are manifested. Interestingly, at the device level, it has been reported that the effects these two mechanisms can have on *JV* curves are sometimes quite similar, and this provides a key point of departure from the traditional solar cell model.[56,73–76]

Regarding terminology, note that we employ the terms "lowest unoccupied molecular orbital" (LUMO) and "highest occupied molecular orbital" (HOMO) throughout this article. This language comes from frontier molecular orbital theory and can be misleading in that orbital energies change with orbital occupation. We retain the language, which is omnipresent in the literature, but it must be remembered that the language only approximates the actual physics.

3.2. Geminate pair recombination effects on organic solar cell response

Experimental and modeling studies[40,73,74,77–80] support the conclusion of a reduced photocurrent (*i.e.*, J_{ph}) yield and, in some cases, J_{ph} dependence on cell voltage, arising from geminate pair recombination. Fig. 5a illustrates how these recombination effects may be manifested, with hypothetical "nonideal" J_{ph} curves represented as simple straight lines. These hypothetical curves are qualitatively consistent with prior studies, demonstrating reduced quantum efficiencies and some photocurrent field dependence.[40,73,74,77–80] Fig. 5a also shows a dark current curve typical of OPVs and an "ideal J_{ph}" curve, which is representative of the scenario in which all geminate pairs dissociate with 100% efficiency, regardless of cell voltage. Based on these ideal and nonideal J_{ph} curves (Fig. 5a), Fig. 5b illustrates how geminate pair photocurrent recombination can lead to losses in the illuminated *JV* curves.[80] Interestingly, the nonzero slope near the y-intercept is a traditional signature of a shunt current loss.[32–34,81] However, here we see another possible cause for this response: incomplete and field-assisted geminate pair dissociation.[73,79,80] In other words, there can be less photogenerated current at weaker fields, thereby leading to reduced fill factor and J_{sc} performance relative to the ideal case (Fig. 5b).[73,79,80,82] We also observe some reduction in V_{oc} from this simple analysis. Experimental cells with low donor–acceptor orbital energy offsets[83,84] typically produce *JV* curves similar to the nonideal cases in Fig. 5b. See Section 3.3 for a discussion of donor–acceptor orbital energy offsets. Note that there is some debate in the field regarding when field-assisted geminate pair dissociation is operative *vs.* when it is field-independent; we address this issue in further detail below. Likewise, bimolecular recombination can result from a variety of sources (*e.g.*, mobility, trap, and cell area effects)[56,69,76,85,86] and can produce quite similar effects on illuminated cell performance (Fig. 5b). Developing a greater understanding of these loss mechanisms is crucial to achieving 10% OPV power conversion efficiencies and beyond.

3.3. The influence of LUMO offset energy on geminate pair dissociation

Fig. 6a sketches the donor–acceptor energy landscape in organic solar cells, including the donor–acceptor offset energy (ΔE_{LUMO}) and bandgap (E_g) in a simple one electron scheme. For state-of-the-art systems, the donor material is typically the primary absorber,[7,22,26,87] and therefore, the bandgap (E_g) of the donor generally determines what photon energies can be absorbed by

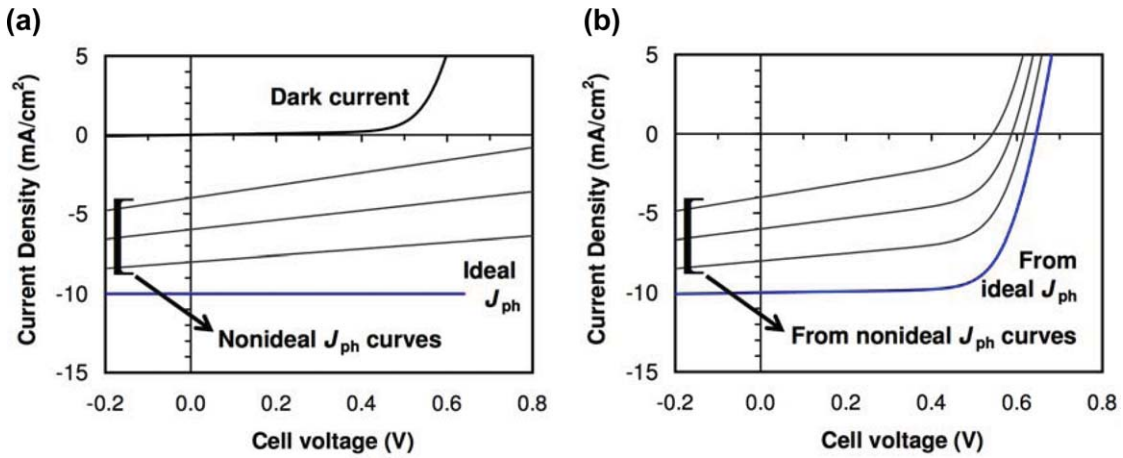

Fig. 5 (a) Typical OPV dark *JV* curve and ideal J_{ph} curve, as well as hypothetical nonideal J_{ph} curves based on geminate pair or bimolecular recombination of the photocurrent only (not accounting for dark current recombination, which is also shown). Note that actual J_{ph} curves are not necessarily linear, and these nonideal curves are used for illustration purposes only. (b) Illustration of how this recombination behavior (nonideal J_{ph} curves) can reduce the photovoltaic performance.

these systems. Similarly, the LUMO offset (ΔE_{LUMO}) between the donor and acceptor (Fig. 6a) is a critical parameter in understanding the geminate pair dissociation dynamics. Note that in systems where the acceptor material absorbs significant light, a similar analysis applies in considering the HOMO offset[88] (ΔE_{HOMO}); for clarity we focus here on ΔE_{LUMO}. The LUMO offset is not only necessary for the initial electron transfer process, but has also been shown to be of crucial importance in promoting geminate pair dissociation and free charge photogeneration.[41,42,66,89,90] Additionally, the body of experimental literature on organic solar cells supports these spectroscopic observations: systems with large ΔE_{LUMO} values (*e.g.*, ~1.0 eV) often display nearly ideal J_{ph} curves,[10,26,48] with geminate pair dissociation quantum efficiencies approaching 100% with high fill factors; the ideal J_{ph} case in Fig. 5a and 5b illustrates this effect. In contrast, systems with more modest ΔE_{LUMO} values (0.2–0.3 eV)[42,83,89,90] exhibit suppressed quantum efficiencies and fill factors; the nonideal J_{ph} cases in Fig. 5a and 5b more accurately depict these effects.

Despite the above considerations, low LUMO offsets are desirable for high overall power conversion efficiencies. For example, previous state-of-the-art cells employed E_g = 2.0 eV and ΔE_{LUMO} = 1.0 eV; in this case, approximately half of the exciton energy is expended in the charge separation process, as in OPVs based on P3HT:PCBM (poly(3-hexylthiophene):6,6-phenyl C_{61}-butyric acid methyl ester).[91,92] Large losses such as this provide a key reason why 10% efficient OPVs have yet to be discovered; therefore, development of models and materials targeting the tradeoff between ΔE_{LUMO} and photocurrent generation are critical for designing efficient OPVs with more modest LUMO offsets.

The enhancement of practical efficiency limits by introducing lower LUMO offsets was previously reported;[3,6,39,43,92,93] the calculated practical efficiency limit data from ref. 92 are presented in Fig. 6b (blue curve), showing how efficiency limits substantially increase for lower LUMO offsets. Note here that E_g is also reoptimized for each ΔE_{LUMO}, as discussed in ref. 74. Record power conversion efficiencies for various ΔE_{LUMO} values are also shown in Fig. 6b (red markers). There is a clear discrepancy between these modeled efficiency limits (blue curve) and actual experimental performance levels at lower LUMO offsets. On the other hand, there appears to be good agreement for larger ΔE_{LUMO} values (~1.0 eV). The mechanism by which the ΔE_{LUMO} affects the dissociation process is a crucial topic of ongoing research.[42] By understanding how to predict the performance tradeoffs in moving to lower LUMO offsets (gray curve, Fig. 6b), we can design materials and architectures that optimize geminate pair dissociation rates and, thus, cell efficiencies at lower LUMO offsets.

Fig. 7 illustrates the significant effects that donor–acceptor energy offsets can have on photocurrent (J_{ph}). These J_{ph} values are calculated from a previously reported method of electron-hole dissociation, originating from work by Arkhipov *et al.*,[94] which models the influence of excess vibrational energy on dissociation yield. For application to BHJ OPVs, this excess energy is taken to be ΔE_{LUMO},[80] instead of the excess photon energy in a pristine conjugated polymer as modeled by Arkhipov *et al.* To highlight specifically the effects of donor–acceptor energy offsets (ΔE_{LUMO} here), all other factors are held constant (including bandgap = 2.0 eV). Interestingly, when ΔE_{LUMO} = 1.0 eV (Fig. 7), J_{ph} is nearly ideal, similar to Fig. 5. Experimental studies of P3HT:PCBM OPV cells, also with ΔE_{LUMO} = 1.0 eV and bandgap = 2.0 eV, yield comparable results.[11,95] On the other hand, the J_{ph} curve for the low energy offset case (ΔE_{LUMO} = 0.3 eV) is substantially limited, specifically due to suppressed geminate charge dissociation efficiency. Low quantum yields such as this are common for low ΔE_{LUMO} systems.[83,84] Typically, when low ΔE_{LUMO} systems are introduced, the suppressed dissociation yield is compensated for by using lower bandgap materials (E_g = ~1.5 eV) to collect more light.[83,96] However, this in turn reduces the cell voltage and overall device efficiency; this result helps to explain why state-of-the-art devices typically have larger bandgaps of E_g = 1.7–1.8 eV.[22,97] It is important to note that bimolecular recombination can further reduce the yields shown in Fig. 7. This is primarily an issue for higher cell voltages when the open circuit voltage is approached; for lower cell

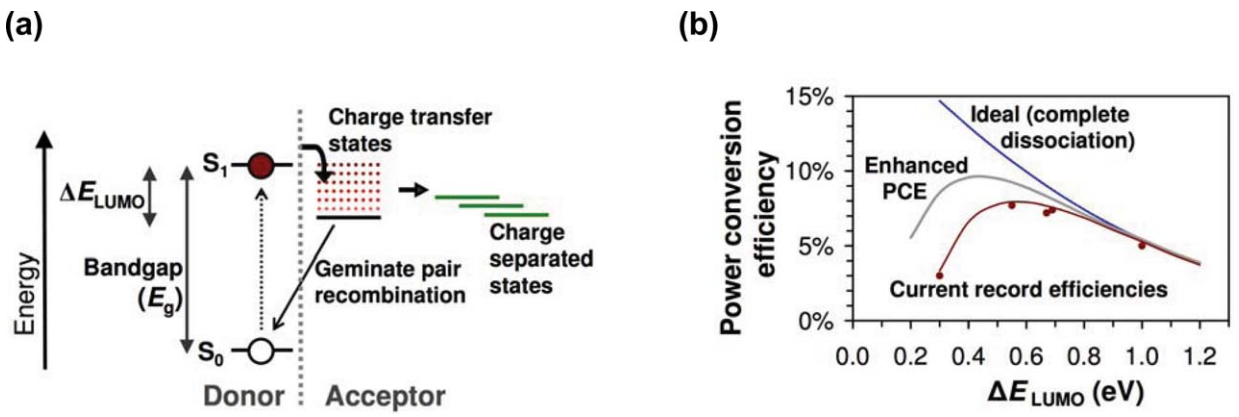

Fig. 6 (a) Organic solar cell energy level diagram, adapted from ref. 45. Regarding terminology, recall that the term "LUMO" comes from frontier molecular orbital theory and is misleading, since orbital energies change with orbital occupation. We employ the language here, as it is standard in the literature, but the language only approximates the actual physics.[45] (b) Record OPV power conversion efficiencies from the literature for the indicated LUMO offsets (red markers, with the line drawn as a guide to the eye), previously reported practical efficiency limits (blue curve),[11,22,83] and hypothetical enhanced power conversion efficiency (PCE) curve (gray curve).

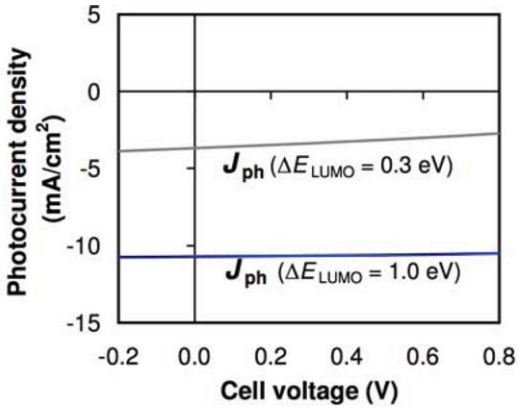

Fig. 7 Simulated J_{ph} curves based upon a previously reported model for electron-hole dissociation.[94] Note the strong influence that the donor–acceptor energy offset (ΔE_{LUMO}) has on photocurrent yield due to limited photogenerated charge dissociation at low energy offsets, such as $\Delta E_{LUMO} = 0.3$ eV. A key challenge for future organic solar cell materials design is to enhance charge dissociation at low energy offsets (*e.g.*, $\Delta E_{LUMO} = \sim 0.2$–$0.3$ eV).[80]

voltages (approaching $V = 0$), it has been demonstrated in well-optimized systems that internal quantum efficiencies approach 100% and that bimolecular recombination therefore approaches zero.[10,11,48]

3.4. Bandgap implications for high efficiency organic solar cells

The above analysis suggests that redshifting OPV bandgaps alone to lower energies (*e.g.*, 1.4–1.5 eV) *vs.* the current state of the art (E_g = 1.7–1.8 eV) – without improving other properties such as reduced exciton binding energy[36,37] or enhanced attempt-to-jump frequency[94] – should only depress *optimal* device efficiency.[80] This is a clear departure for OPVs from the seminal work by Shockley and Queisser that demonstrated in traditional *p-n* junction inorganic solar cells an optimal $E_g = \sim 1.4$ eV.[27] This divergence from Shockley-Queisser behavior is due to organic solar cells requiring an offset energy between the donor and acceptor materials for exciton and geminate pair dissociation – with a larger offset, a larger bandgap is also necessary.[39,92] Current state-of-the-art materials typically exhibit ΔE_{LUMO} = 0.55–0.7 eV,[22,97] which are offset energies that significantly limit overall power conversion efficiency.[3,6,43,92] Therefore, a fundamental design challenge for OPVs is to achieve high charge dissociation yields at low energy offsets (*e.g.*, $\Delta E_{LUMO} = 0.3$ eV). If this is achieved, then the optimal bandgap should move to lower values (*e.g.*, ~1.6–1.7 eV).[92] Two key approaches to address this challenge are to reduce the exciton binding energy[94] and enhance the local mobility[79] at the donor–acceptor interface. Importantly, current generation devices already approach near optimal efficiencies (~8–9%) achievable *via* energy level tuning alone. Therefore, without the introduction of new generations of materials with higher local mobilities (at the donor–acceptor interface) or lower exciton binding energies, single layer OPV power conversion efficiencies are projected to plateau near current record levels of ~8–9%, based upon applying the Arkhipov *et al.* model to OPVs.[94] However, through improved materials design, efficiencies >10% are well within reach. Note several studies have taken various approaches to the question of maximum practical efficiency limits and optimal bandgap in OPVs, with results ranging from PCE estimations of ~8–11% and optimal bandgap energies of ~1.4–1.5 eV.[3,39,43] We expect optimal bandgap energies to be somewhat greater (~1.6–1.7 eV) in new generation high efficiency OPVs because some of the energy from ΔE_{LUMO} is lost due to thermal dissipation[98] before geminate pair dissociation is complete – this in turn requires somewhat larger values of ΔE_{LUMO} and E_g.[44] Finally, note that while in principle there should be a single optimal bandgap energy, there is generally a relatively wide shoulder of ±~0.2–0.3 eV, such that a range of bandgap energies can still produce relatively high performing OPVs. For example, Scharber *et al.* calculate that a bandgap range of 0.65 eV produces a variation of only ~1% in power conversion efficiency.[3]

4. Blocking layer effects: field-dependent photocurrent recombination at electrode interfaces

4.1. Background on interfacial layers

Interfacial layers at electrode/active layer interfaces (Fig. 1) can provide significant efficiency enhancements in organic solar cells,[6,11,26,35,99–119] and various mechanisms are proposed for different systems. Two mechanisms frequently discussed in the literature are that these layers: (a) increase photocurrent extraction by reducing extraction barrier heights (*i.e.*, "transport" layers) and (b) reduce recombination at the electrodes by serving as "blocking" layers.[99–101] At the anode, where holes are collected, the first mechanism is to enhance hole extraction, and the layer is commonly termed a "hole transport layer" (HTL).[99–101] When discussing the second mechanism at the anode, where electron injection is unfavorable due to recombination with holes, the layer is commonly termed an "electron blocking layer" (EBL).[99–101]

Regarding deviations from the conventional solar cell model (eqn (1)), we focus here on the blocking layer mechanism while keeping in mind that both mechanisms can potentially play important roles. There is strong evidence that blocking layers are one key means to enhance BHJ organic solar cell efficiency.[99–101,105,119–121] However, complete models explaining the details of the improvements are still under development. Below we show how the blocking layer mechanism provides a feature of organic solar cell behavior deviating from conventional inorganic models. In particular, while conventional approaches commonly take the photocurrent term (J_{ph} in Fig. 2a and eqn (1)) as field-independent, we show below how the *absence* of an EBL can lead to strong photocurrent field dependence due to competition between drift and diffusion currents at the anode interface.

4.2. Anode photocurrent (J_{ph}) recombination

Fig. 1 provides an illustration of how blocking layers are important in BHJ OPVs: since both the donor (hole-conducting) and acceptor (electron-conducting) phases are typically in contact with both electrodes, recombination at these interfaces becomes a potential loss mechanism. For example, if both holes and electrons are extracted to the anode, then immediate recombination is expected; therefore, the goal at this layer is to

only extract holes.[99–101] Due to the blend morphology of the BHJ system, allowing both phases to be in contact with each electrode, this loss mechanism is unique to BHJ organic solar cells and other systems with similar active layer morphologies. Note that for clarity, we concentrate on the anode interface here; the same analysis applies to the cathode interface.

Fig. 8 provides a more detailed picture of this recombination process in terms of a proposed competition between electron diffusion (J_{diff}) and drift (J_{drift}, or field-driven) current densities. In a typical photovoltaic cell, the built-in electric field helps drive electrons to the cathode (to the right in Fig. 8) and holes to the anode (to the left in Fig. 8). Furthermore, the cell voltage works against the built-in field under typical operating conditions; *i.e.*, when the cell voltage increases, the electric field decreases, and vice versa. Across the active layer, the average electric field = $(V_0 - V)/d$, where V_0 is the built-in voltage, and d is the active layer thickness.[61] Therefore, for low cell voltages (*e.g.*, ~0.1 V), the electric field is relatively strong, increasing the drift current and driving charge carriers to their respective electrodes – holes to the anode, electrons to the cathode. For high cell voltages near the open circuit voltage, the average electric field is relatively weak, enabling the diffusion current to compete with the drift current. Fig. 8a shows the case where the electron drift current predominates over the diffusion current, and Fig. 8b shows the opposite case, where the diffusion current predominates at the anode interface. When electron diffusion dominates, more electrons move to the "wrong" electrode, which is also populated by holes, leading to recombination losses. Note that the electric field will not be perfectly constant throughout the device – the morphological and electronic landscape will create some variations. However, under operating voltages, lowering the cell voltage increases the average electric field, and vice versa.

EBLs are designed to prevent electron extraction at the anode, regardless of field strength. Fig. 8c shows this design: the LUMO level of the EBL (or conduction band minimum in the case of inorganic EBLs) is positioned sufficiently high to suppress nearly all electron diffusion current to the anode.[99–101] Additionally, the EBL HOMO level (or valence band maximum for inorganic EBLs) is positioned to align with the HOMO level of the donor material and the anode work function to promote hole extraction to the anode. Therefore, regardless of strong or weak field strengths, an EBL is ideally designed to suppress anode recombination by promoting hole extraction and eliminating electron extraction – *i.e.*, acting as a filter for holes.

4.3. Implications for BHJ organic solar cell models

The behaviors discussed above have significant implications for BHJ organic solar cell device models, requiring a modified mechanistic picture and differentiation from conventional theory. Traditionally, the photocurrent (J_{ph}) is taken to be independent of cell voltage and electric field – *i.e.*, a horizontal line as shown in Fig. 5a. Likewise, in the presence of an EBL, the J_{ph} curve is taken as this ideal J_{ph} curve (Fig. 9, horizontal line). It is important to note here that to highlight the EBL mechanism, we ignore other forms of photocurrent recombination; in reality, these sources, such as bimolecular and geminate pair recombination, typically have important effects. In this scenario, the J_{ph} curve is ideal because, regardless of field strength, the EBL eliminates the electron diffusion current to the anode and thus effectively eliminates anode electron-hole recombination. Without the EBL, the electron diffusion current to the anode dominates the drift current at weak field strengths (Fig. 8b),

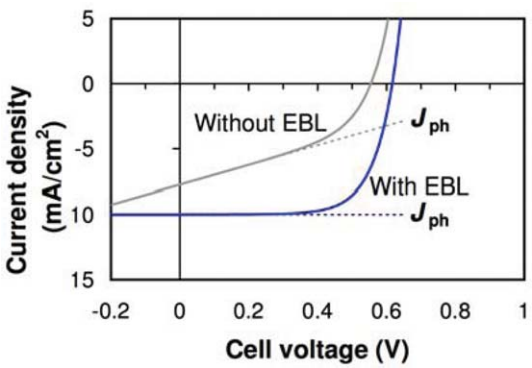

Fig. 9 Current density *vs.* cell voltage (JV) curves for hypothetical OPV cases with and without an EBL. Similar JV responses for these two cases have been demonstrated experimentally.[120–122] The suppressed performance in the absence of an EBL is due to charge recombination at the anode. Note that actual J_{ph} curves are not necessarily linear, and these curves are used to illustrate the effects of EBLs.

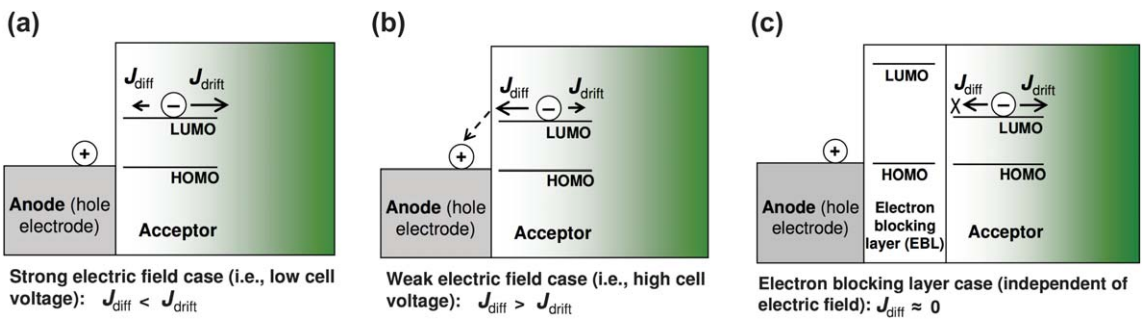

Fig. 8 Diagram of the interface between the electron acceptor and anode (the hole-collecting electrode, or transparent electrode in Fig. 1). Three cases are described: (a) the absence of an electron blocking layer (EBL) for strong electric field (low cell voltage), (b) the absence of an EBL for a weak electric field (high cell voltage), and (c) the presence of an EBL, regardless of the field strength; here the EBL suppresses the recombination current even for weak net fields, when diffusion currents would otherwise dominate and enhance anode recombination.

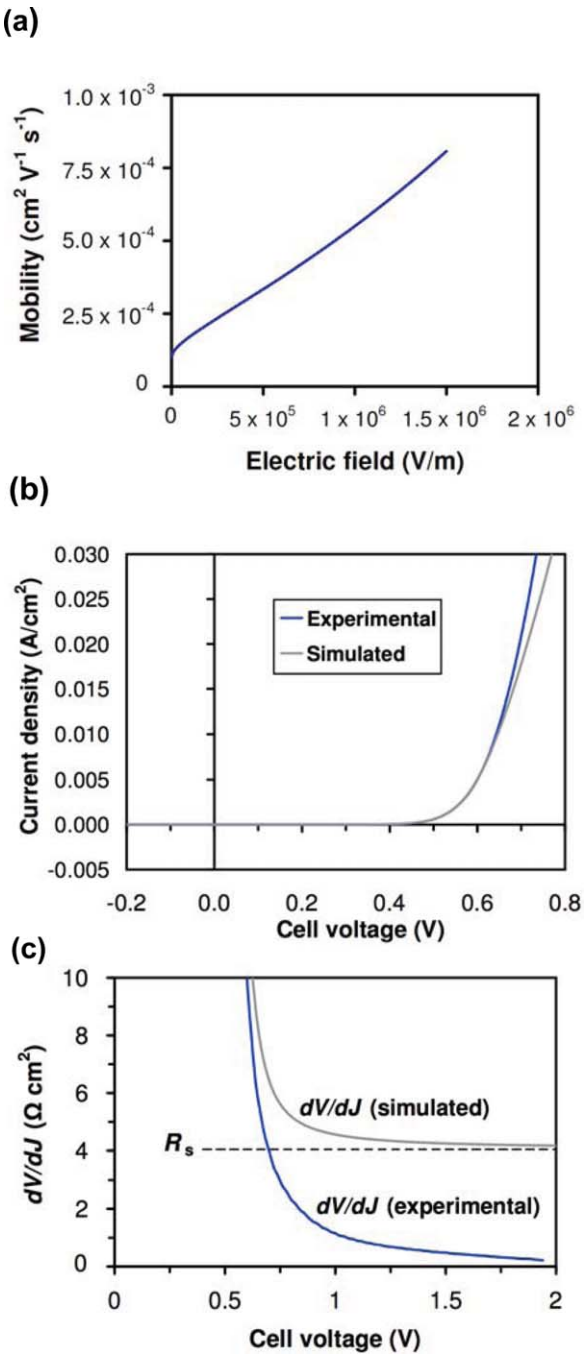

Fig. 10 (a) Illustration of the Poole-Frenkel effect (eqn (3)) on OPV active layer mobility, assuming a dielectric constant = 4, $T = 298$ K, and a zero field mobility = 1×10^{-4} cm^2 V^{-1} s^{-1}. The range of electric fields shown here are over a typical cell voltage test range (~1 V), showing how mobility and, thus, resistance vary significantly with cell voltage. Note that the nonlinear, exponential features of this curve are more apparent when a larger voltage range is considered (*e.g.*, ~10 V). (b) Experimental dark *JV* data for a P3HT:PCBM OPV cell, previously reported in ref. 105, and simulated data for the same cell. The simulated data are based on fitting the experimental data to eqn (1); there is good agreement of both curves except at high voltages due to the voltage-dependent R_s value. (c) The differential resistance *dV/dJ vs.* cell voltage for the simulated and experimental curves in Fig. 10b. The R_s value is from fitting the experimental data to eqn (1) and serves as a lower limit for the simulated *dV/dJ* value, in accordance with traditional *p-n* junction inorganic solar cell theory. The experimental *dV/dJ* data fall well below this limit due to enhanced conductivities at higher cell voltages, and demonstrate the breakdown of traditional theory for determining R_s at high cell voltages. Note that average field strength is zero at V_0 because $F = (V_0 - V)/d$. Therefore, at both low ($V < V_0$) and high ($V > V_0$) cell voltages, the average electric field increases across the cell.

leading to current loss at high cell voltages; likewise, at strong fields, electron drift current *away* from the anode dominates (Fig. 8a), and the anode photocurrent recombination is greatly reduced. This behavior creates a unique J_{ph} voltage dependence and can manifest itself as a substantial V_{oc} reduction (Fig. 9). These V_{oc} enhancements have been associated with a wide array of interfacial layers.[99–101,105,119–121] Importantly, J_{sc} is affected if the diffusion (recombination) current still competes with the drift current at $V = 0$. Fig. 9 illustrates why V_{oc} reduction can be crucial: without the blocking layer, more photocurrent is lost at increasing cell voltages, and therefore, zero net current is achieved at a lower voltage, thereby lowering the V_{oc} – *i.e.*, when recombination current offsets generated photocurrent. Ongoing research is focusing on modeling and predicting these interesting photocurrent recombination dynamics.

As outlined earlier, interfacial layers serve purposes beyond the blocking layer mechanisms. Notably, it has been argued that materials such as MoO_3 promote hole transport at the anode, thereby also providing V_{oc} enhancements.[106–112] Note that transport layers such as these are potentially useful for any solar cell device that requires charge injection[123] from one layer to another, not just BHJ OPVs. More complex models can be developed to account for the benefits of these layers, by decoupling blocking and transport layer effects. This is also an area ripe for development of experimental characterization techniques that differentiate between the two mechanisms. Finally, in addition to these mechanisms, important considerations for interfacial layer design include: optical transparency (particularly for wavelengths absorbed by the active layer), passivation of trap sites, and templating effects on active layer microstructure.[99–101]

5. Series resistance: Electric field and cell area dependence

5.1. Field-dependent mobility and resistance

Traditionally, *p-n* junction solar cell models assume that series resistance[32,34,124] is independent of electric field strength. Therefore, when cell voltage varies, series resistance is assumed to remain constant (eqn (1)). However, in organic semiconductors, this model breaks down due to their field-dependent conductivities – conductivity significantly increases with field strength. The Poole-Frenkel formulation for charge mobility helps explain this result:

$$\mu \propto \exp\left[\frac{e^{3/2}}{2k_B T}\left(\frac{E}{\pi\varepsilon_o\varepsilon_r}\right)^{1/2}\right], \quad (3)$$

where μ is mobility, e the elementary charge, k_B Boltzmann's constant, T temperature, E the electric field strength, ε_o the vacuum permittivity, and ε_r the dielectric constant.[125,126] This

relationship essentially shows how mobility increases with increasing field strength. Given that conductivity is the product of mobility, charge density, and the elementary charge ($\sigma = \mu Ne$), conductivity and thus resistivity have important exponential relationships with $E^{1/2}$. Furthermore, the average electric field across the cell scales linearly with cell voltage ($(V_0 - V)/d$), and therefore, cell voltage is a key determinant governing the internal cell resistance. The importance of the Poole-Frenkel effect for organic semiconductor mobilities has been extensively discussed.[125,126] The impact of the Poole-Frenkel effect on mobility is shown graphically in Fig. 10a, applying eqn (3) and assuming a dielectric constant = 4. In addition to the Poole-Frenkel effect, charge carrier densities also increase with cell voltage.[126] Since conductivity is determined by the product of mobility and charge carrier density, this effect makes the voltage dependence of R_s even more significant.

The influence of cell voltage on R_s is demonstrated in Fig. 10b and 10c. Previously reported JV dark data for a well-studied P3HT:PCBM OPV system are shown in Fig. 10b.[105] We extracted the parameters in eqn (1) *via* a least-squares fit applied to this experimental JV data set over a typical operating voltage range of 0.2–0.6 V. The resulting parameters are: $J_0 = 1.54 \times 10^{-9}$ A/cm^2, $R_s = 4.05\ \Omega$ cm^2, $n = 1.50$, $R_{sh} = 3.69 \times 10^6\ \Omega$ cm^2. Over the range from $V = 0$ to typical operating voltages of this cell, ~0.5–0.6 V, there is typically good agreement between experimental and simulated (based on eqn (1)) data, demonstrating the usefulness of traditional *p-n* theory in studying OPVs. However, at high cell voltages, the experimental and simulated curves diverge, evidencing a breakdown of the model. This divergence is also shown in Fig. 10c, where the differential resistance curves (dV/dJ) are presented for the experimental and simulated cases. Additionally, the fitted value for R_s (4.05 Ω cm^2) is shown in Fig. 10c.

This deviation between observed and predicted behavior at high cell voltage has important implications for describing OPV response. It is common practice to estimate R_s by determining dV/dJ in the range from V_{oc} up to high cell voltages (~1–2V). The reason for this approach, according to traditional theory,[32] is that at high voltages the slope of the JV curve is primarily determined by R_s – as demonstrated by the simulated dV/dJ and R_s curves merging for $V > 1$ V. However, the field-dependent conductivities in OPVs essentially make determining R_s a moving target. What voltage specifically should one use in determining R_s? If dV/dJ is calculated at a high voltage, the resistance is artificially and significantly reduced by an order of magnitude or more (Figs. 10a and 10c). Since the resistance near typical operating voltages and V_{oc} (for P3HT:PCBM, this range is ~0.4–0.6 V) is more relevant, the JV data should be evaluated at these lower voltages; however, dV/dJ is no longer determined by R_s at these voltages, as evidenced by the rapidly increasing dV/dJ values on the left hand side of Fig. 10c. This is simply because the solar cell diode current strongly influences dV/dJ at these voltages. Therefore, to address this complication, it is crucial to extract R_s by fitting the data near the operating voltage of the cell. Ideally, this fitting process would also include the Poole-Frenkel and other field-dependent effects, although the drawback of doing so is that further fit parameters are being added, increasing the complexity and decreasing the accuracy of the parameter extraction.

Ultimately, the field-dependent conductivities in organic semiconductors complicate the accurate determination of R_s in OPVs. It is evident from Fig. 10c, that calculations of dV/dJ can lead to widely varying results depending the voltage used. A recommended means of reducing the influence of field strength is to fit the traditional model (eqn (1)) near the operating voltage of the cell over a relatively tight range (~400 mV). Applying other techniques including impedance[127] and time-of-flight (TOF) spectroscopy[48] may provide methods for supporting the accuracy of these extracted R_s values. Care should also be taken in measuring mobilities, given the strong dependence on electric field (Fig. 10a).

5.2. Area dependence of series resistance

Finally, cell area can have an important impact on series resistance in organic solar cells. These devices typically have an anode (transparent electrode) based on indium tin oxide (ITO) or a related transparent conducting oxide (TCO) as the anode material (Fig. 1). These layers must be both transparent and conductive; however, conductivities for the most conductive TCOs can be more than an order of magnitude lower than are typical metal conductivities.[58] As a result, when current is collected by the transparent electrode, resistance losses are substantial unless the cell area is small (*i.e.*, cell area $\ll$ 1 cm^2). These effects were recently reported in ref. 43 and are shown in Fig. 11 for a simulated high efficiency OPV scenario. While efficiencies for very small cells (area < 0.1 cm^2) show little sensitivity to anode conductivity, such cell areas generally are not useful in energy production.[26,58] For more practical cell areas (*e.g.*, $\geq$1 cm^2), there is substantial sensitivity to cell area. This is a direct result of the series resistance (Fig. 11) being a function of cell area in organic solar cells. At moderate cell areas (*e.g.*, 1 cm^2), the series resistance is significantly dependent upon the anode material selection, highlighting the importance of high conductivity transparent conductors for organic solar cells.[58] This effect is not limited to OPVs; other inorganic thin film solar cells requiring transparent conductors also exhibit this effect. These resistance losses can be reduced by closely spacing current collectors on the transparent electrode material. However, this approach introduces practical drawbacks of added cost and

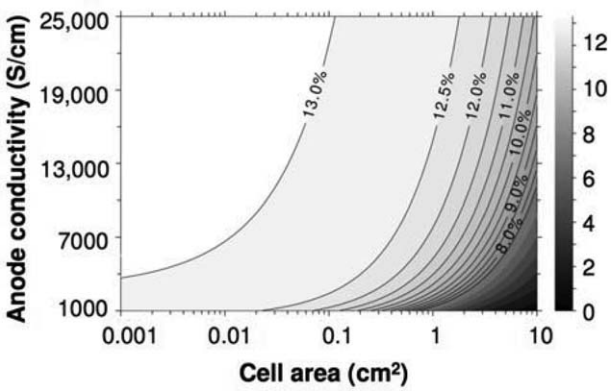

Fig. 11 The effects anode (transparent electrode) conductivity and cell area have on power conversion efficiency due to internal resistance losses. This figure is reproduced with permission from ref. 43.

blocking some incoming radiation. Note that in addition to cell area affecting series resistance, recent reports have also shown that cell area can influence OPV performance due to light scattering at the cell perimeter[128] and enhanced recombination currents.[86]

6. Conclusions

Traditional inorganic solar cell models have offered significant insight into organic solar cell response; however, addressing key points of departure from the traditional models is essential for understanding and accurately modeling OPV performance. The significant electronic and structural differences between organic and traditional silicon solar cells require modifications of conventional modeling approaches. The large exciton binding energies in organic semiconductors translate to new loss mechanisms, notably geminate pair (charge transfer state) recombination pathways. Important areas of future research include the development of OPVs with low donor–acceptor energy offsets (*e.g.*, ~0.2–0.3 eV) that exhibit low geminate pair recombination rates. Proposed strategies to achieve this include enhanced local mobility at the donor–acceptor interface, reduced exciton binding energies, and enhanced electron–phonon coupling at the interface – using the vibrational energy at the donor–acceptor interface more efficiently to enhance geminate pair dissociation. Device architecture is also an important issue: the tortuous charge transport pathways within BHJ OPV active layers provide opportunities for electron-hole collision and recombination before the charges can be harvested at their respective electrodes; future research on the development of more ordered architectures will be important in reducing this recombination pathway.[6,129] These recombination processes lead to photocurrent-voltage dependences not found in the traditional solar cell model. Additionally, when both donor and acceptor materials are in contact with each cell electrode, further photocurrent recombination sources are introduced, creating another source of J_{ph} voltage dependence and the need for selective, blocking layer electrode contacts. Finally, the strong dependence of OPV series resistance on field strength and cell area requires revisions to traditional models. Accounting for key differences such as these provides a new perspective when applying traditional inorganic solar cell models to identify crucial bottlenecks in organic solar cell performance.

Acknowledgements

We thank the U.S. DOE-BES Argonne-Northwestern Solar Energy Research Center (ANSER), an Energy Frontier Research Center (Award DE-SC0001059), and a Link Foundation Energy Fellowship for support of this research. We thank M. Lundstrom, A. Alam, M. McGehee, B. Savoie, and S. Dongaonkar for useful discussions.

References

1 C. W. Tang, *Appl. Phys. Lett.*, 1986, **48**, 183–185.
2 W. L. Ma, C. Y. Yang, X. Gong, K. Lee and A. J. Heeger, *Adv. Funct. Mater.*, 2005, **15**, 1617–1622.
3 M. C. Scharber, D. Wuhlbacher, M. Koppe, P. Denk, C. Waldauf, A. J. Heeger and C. L. Brabec, *Adv. Mater.*, 2006, **18**, 789–794.
4 C. J. Brabec, N. S. Sariciftci and J. C. Hummelen, *Adv. Funct. Mater.*, 2001, **11**, 15–26.
5 C. J. Brabec, *Sol. Energy Mater. Sol. Cells*, 2004, **83**, 273–292.
6 K. M. Coakley and M. D. McGehee, *Chem. Mater.*, 2004, **16**, 4533–4542.
7 B. C. Thompson and J. M. J. Frechet, *Angew. Chem., Int. Ed.*, 2008, **47**, 58–77.
8 B. Kippelen and J. L. Bredas, *Energy Environ. Sci.*, 2009, **2**, 251–261.
9 S. E. Gledhill, B. Scott and B. A. Gregg, *J. Mater. Res.*, 2005, **20**, 3167–3179.
10 S. H. Park, A. Roy, S. Beaupre, S. Cho, N. Coates, J. S. Moon, D. Moses, M. Leclerc, K. Lee and A. J. Heeger, *Nat. Photonics*, 2009, **3**, 297–303.
11 J. Y. Kim, S. H. Kim, H. H. Lee, K. Lee, W. L. Ma, X. Gong and A. J. Heeger, *Adv. Mater.*, 2006, **18**, 572–576.
12 G. Yu, J. Gao, J. C. Hummelen, F. Wudl and A. J. Heeger, *Science*, 1995, **270**, 1789–1791.
13 C. Waldauf, M. C. Scharber, P. Schilinsky, J. A. Hauch and C. J. Brabec, *J. Appl. Phys.*, 2006, **99**, 104503.
14 S. E. Shaheen, C. J. Brabec, N. S. Sariciftci, F. Padinger, T. Fromherz and J. C. Hummelen, *Appl. Phys. Lett.*, 2001, **78**, 841–843.
15 J. G. Xue, S. Uchida, B. P. Rand and S. R. Forrest, *Appl. Phys. Lett.*, 2004, **84**, 3013–3015.
16 P. Peumans, A. Yakimov and S. R. Forrest, *J. Appl. Phys.*, 2003, **93**, 3693–3723.
17 P. Peumans and S. R. Forrest, *Appl. Phys. Lett.*, 2001, **79**, 126–128.
18 W. Z. Cai, X. Gong and Y. Cao, *Sol. Energy Mater. Sol. Cells*, 2010, **94**, 114–127.
19 T. Ameri, G. Dennler, C. Lungenschmied and C. J. Brabec, *Energy Environ. Sci.*, 2009, **2**, 347–363.
20 J. Y. Kim, K. Lee, N. E. Coates, D. Moses, T. Q. Nguyen, M. Dante and A. J. Heeger, *Science*, 2007, **317**, 222–225.
21 Y. Y. Liang, D. Q. Feng, Y. Wu, S. T. Tsai, G. Li, C. Ray and L. P. Yu, *J. Am. Chem. Soc.*, 2009, **131**, 7792–7799.
22 Y. Y. Liang, Z. Xu, J. B. Xia, S. T. Tsai, Y. Wu, G. Li, C. Ray and L. P. Yu, *Adv. Mater.*, 2010, **22**, E135–E138.
23 M. A. Green, K. Emery, Y. Hishikawa and W. Warta, *Prog. Photovoltaics*, 2011, **19**, 84–92.
24 R. F. Service, *Science*, 2011, **332**, 293.
25 R. W. Birkmire and E. Eser, *Annu. Rev. Mater. Sci.*, 1997, **27**, 625–653.
26 G. Dennler, M. C. Scharber and C. J. Brabec, *Adv. Mater.*, 2009, **21**, 1323–1338.
27 W. Shockley and H. J. Queisser, *J. Appl. Phys.*, 1961, **32**, 510–519.
28 C. T. Sah, R. N. Noyce and W. Shockley, *Proc. IRE*, 1957, **45**, 1228–1243.
29 W. Shockley and W. T. Read, *Phys. Rev.*, 1952, **87**, 835–842.
30 W. Shockley, *AT&T Tech. J.*, 1949, **28**, 435–489.
31 R. N. Hall, *Phys. Rev.*, 1952, **87**, 387–387.
32 S. M. Sze, *Physics of Semiconductor Devices*, Wiley-Interscience, New York, NY, USA, 1981.
33 M. A. Green, *Solar Cells: Operating Principles, Technology, and System Applications*, Prentice-Hall, Inc., Englewood Cliffs, NJ, USA, 1982.
34 A. L. Fahrenbruch and R. H. Bube, *Fundamentals of Solar Cells*, Academic Press, New York, NY, USA, 1983.
35 M. Helgesen, R. Sondergaard and F. C. Krebs, *J. Mater. Chem.*, 2010, **20**, 36–60.
36 J. J. M. Halls, J. Cornil, D. A. dos Santos, R. Silbey, D. H. Hwang, A. B. Holmes, J. L. Bredas and R. H. Friend, *Phys. Rev. B: Condens. Matter*, 1999, **60**, 5721–5727.
37 S. Barth and H. Bassler, *Phys. Rev. Lett.*, 1997, **79**, 4445–4448.
38 K. Hummer and C. Ambrosch-Draxl, *Phys. Rev. B: Condens. Matter Mater. Phys.*, 2005, **71**, 081202.
39 D. Veldman, S. C. J. Meskers and R. A. J. Janssen, *Adv. Funct. Mater.*, 2009, **19**, 1939–1948.
40 V. D. Mihailetchi, H. Xie, B. de Boer, L. J. A. Koster and P. W. M. Blom, *Adv. Funct. Mater.*, 2006, **16**, 699–708.
41 H. Ohkita, S. Cook, Y. Astuti, W. Duffy, S. Tierney, W. Zhang, M. Heeney, I. McCulloch, J. Nelson, D. D. C. Bradley and J. R. Durrant, *J. Am. Chem. Soc.*, 2008, **130**, 3030–3042.
42 T. M. Clarke and J. R. Durrant, *Chem. Rev.*, 2010, **110**, 6736–6767.
43 L. J. A. Koster, V. D. Mihailetchi and P. W. M. Blom, *Appl. Phys. Lett.*, 2006, **88**, 093511.

44 R. D. Pensack and J. B. Asbury, *J. Phys. Chem. Lett.*, 2010, **1**, 2255–2263.
45 J. L. Brédas, J. E. Norton, J. Cornil and V. Coropceanu, *Acc. Chem. Res.*, 2009, **42**, 1691–1699.
46 X. Y. Zhu, Q. Yang and M. Muntwiler, *Acc. Chem. Res.*, 2009, **42**, 1779–1787.
47 J. J. M. Halls, K. Pichler, R. H. Friend, S. C. Moratti and A. B. Holmes, *Appl. Phys. Lett.*, 1996, **68**, 3120–3122.
48 G. Li, V. Shrotriya, J. S. Huang, Y. Yao, T. Moriarty, K. Emery and Y. Yang, *Nat. Mater.*, 2005, **4**, 864–868.
49 S. Shoaee, M. P. Eng, E. Espildora, J. L. Delgado, B. Campo, N. Martin, D. Vanderzande and J. R. Durrant, *Energy Environ. Sci.*, 2010, **3**, 971–976.
50 C. R. McNeill, S. Westenhoff, C. Groves, R. H. Friend and N. C. Greenham, *J. Phys. Chem. C*, 2007, **111**, 19153–19160.
51 X. Yang, J. Loos, S. C. Veenstra, W. J. H. Verhees, M. M. Wienk, J. M. Kroon, M. A. J. Michels and R. A. J. Janssen, *Nano Lett.*, 2005, **5**, 579–583.
52 Y. Kim, S. Cook, S. M. Tuladhar, S. A. Choulis, J. Nelson, J. R. Durrant, D. D. C. Bradley, M. Giles, I. McCulloch, C. S. Ha and M. Ree, *Nat. Mater.*, 2006, **5**, 197–203.
53 N. Tessler, Y. Preezant, N. Rappaport and Y. Roichman, *Adv. Mater.*, 2009, **21**, 2741–2761.
54 A. J. Heeger, *Chem. Soc. Rev.*, 2010, **39**, 2354–2371.
55 N. C. Cates, R. Gysel, Z. Beiley, C. E. Miller, M. F. Toney, M. Heeney, I. McCulloch and M. D. McGehee, *Nano Lett.*, 2009, **9**, 4153–4157.
56 P. Schilinsky, C. Waldauf, J. Hauch and C. J. Brabec, *J. Appl. Phys.*, 2004, **95**, 2816–2819.
57 M. D. Perez, C. Borek, S. R. Forrest and M. E. Thompson, *J. Am. Chem. Soc.*, 2009, **131**, 9281–9286.
58 J. D. Servaites, S. Yeganeh, T. J. Marks and M. A. Ratner, *Adv. Funct. Mater.*, 2010, **20**, 97–104.
59 W. J. Potscavage, S. Yoo and B. Kippelen, *Appl. Phys. Lett.*, 2008, **93**, 193308.
60 N. C. Giebink, G. P. Wiederrecht, M. R. Wasielewski and S. R. Forrest, *Phys. Rev. B*, 2010, **82**.
61 L. J. A. Koster, E. C. P. Smits, V. D. Mihailetchi and P. W. M. Blom, *Phys. Rev. B: Condens. Matter Mater. Phys.*, 2005, **72**, 9.
62 R. A. Marsh, C. Groves and N. C. Greenham, *J. Appl. Phys.*, 2007, **101**, 083509.
63 J. Cuiffi, T. Benanti, W. J. Nam and S. Fonash, *Appl. Phys. Lett.*, 2010, **96**, 143307.
64 C. G. Shuttle, R. Hamilton, B. C. O'Regan, J. Nelson and J. R. Durrant, *Proc. Natl. Acad. Sci. U. S. A.*, 2010, **107**, 16448–16452.
65 J. Nelson, *The Physics of Solar Cells*, Imperial College Press, London, England, 2003.
66 T. M. Clarke, A. M. Ballantyne, J. Nelson, D. D. C. Bradley and J. R. Durrant, *Adv. Funct. Mater.*, 2008, **18**, 4029–4035.
67 R. A. Street, S. Cowan and A. J. Heeger, *Phys. Rev. B*, 2010, **82**.
68 J. M. Hodgkiss, A. R. Campbell, R. A. Marsh, A. Rao, S. Albert-Seifried and R. H. Friend, *Phys. Rev. Lett.*, 2010, **104**.
69 I. A. Howard, J. M. Hodgkiss, X. P. Zhang, K. R. Kirov, H. A. Bronstein, C. K. Williams, R. H. Friend, S. Westenhoff and N. C. Greenham, *J. Am. Chem. Soc.*, 2010, **132**, 328–335.
70 M. Hilczer and M. Tachiya, *J. Phys. Chem. C*, 2010, **114**, 6808–6813.
71 C. Deibel, *Phys. Status Solidi A*, 2009, **206**, 2731–2736.
72 C. Deibel, A. Wagenpfahl and V. Dyakonov, *Phys. Status Solidi RRL*, 2008, **2**, 175–177.
73 R. A. Marsh, J. M. Hodgkiss and R. H. Friend, *Adv. Mater.*, 2010, **22**, 3672–3676.
74 T. Offermans, S. C. J. Meskers and R. A. J. Janssen, *Proc. SPIE–Int. Soc. Opt. Eng.*, 2005, **5938**, 593812.
75 V. D. Mihailetchi, H. X. Xie, B. de Boer, L. J. A. Koster and P. W. M. Blom, *Adv. Funct. Mater.*, 2006, **16**, 699–708.
76 L. J. A. Koster, V. D. Mihailetchi and P. W. M. Blom, *Appl. Phys. Lett.*, 2006, **88**, 052104.
77 V. D. Mihailetchi, L. J. A. Koster, J. C. Hummelen and P. W. M. Blom, *Phys. Rev. Lett.*, 2004, **93**.
78 P. W. M. Blom, V. D. Mihailetchi, L. J. A. Koster and D. E. Markov, *Adv. Mater.*, 2007, **19**, 1551–1566.
79 D. Veldman, O. Ipek, S. C. J. Meskers, J. Sweelssen, M. M. Koetse, S. C. Veenstra, J. M. Kroon, S. S. van Bavel, J. Loos and R. A. J. Janssen, *J. Am. Chem. Soc.*, 2008, **130**, 7721–7735.
80 J. D. Servaites, B. M. Savoie, J. Brink, T. J. Marks and M. A. Ratner, (in preparation).
81 S. Dongaonkar, J. D. Servaites, G. M. Ford, S. Loser, J. Moore, R. M. Gelfand, H. Mohseni, H. W. Hillhouse, R. Agrawal, M. A. Ratner, T. J. Marks, M. S. Lundstrom and M. A. Alam, *J. Appl. Phys.*, 2010, **108**, 124509–124510.
82 P. Peumans and S. R. Forrest, *Chem. Phys. Lett.*, 2004, **398**, 27–31.
83 A. B. Tamayo, X. D. Dang, B. Walker, J. Seo, T. Kent and T. Q. Nguyen, *Appl. Phys. Lett.*, 2009, **94**, 103301.
84 X. Gong, M. Tong, F. G. Brunetti, J. Seo, Y. Sun, D. Moses, F. Wudl and A. J. Heeger, *Adv. Mater.*, 2011, **23**, 2272–2277.
85 T. M. Clarke, F. C. Jamieson and J. R. Durrant, *J. Phys. Chem. C*, 2009, **113**, 20934–20941.
86 W.-I. Jeong, J. Lee, S.-Y. Park, J.-W. Kang and J.-J. Kim, *Adv. Funct. Mater.*, 2011, **21**, 343–347.
87 J. Hou, H.-Y. Chen, S. Zhang, R. I. Chen, Y. Yang, Y. Wu and G. Li, *J. Am. Chem. Soc.*, 2009, **131**, 15586–15587.
88 M. L. Zhang, H. Wang and C. W. Tang, *Appl. Phys. Lett.*, 2010, **97**, 143503.
89 T. M. Clarke, A. M. Ballantyne, S. Tierney, M. Heeney, W. Duffy, I. McCulloch, J. Nelson and J. R. Durrant, *J. Phys. Chem. C*, 2010, **110**, 6736–6767.
90 S. Shoaee, T. M. Clarke, C. Huang, S. Barlow, S. R. Marder, M. Heeney, I. McCulloch and J. R. Durrant, *J. Am. Chem. Soc.*, 2010, **132**, 12919–12926.
91 F. Yang, M. Shtein and S. R. Forrest, *Nat. Mater.*, 2004, **4**, 37–41.
92 J. D. Servaites, M. A. Ratner and T. J. Marks, *Appl. Phys. Lett.*, 2009, **95**, 163302.
93 B. P. Rand, D. P. Burk and S. R. Forrest, *Phys. Rev. B: Condens. Matter Mater. Phys.*, 2007, **75**, 115327.
94 V. I. Arkhipov, E. V. Emelianova and H. Bässler, *Phys. Rev. Lett.*, 1999, **82**, 1321.
95 G. Li, V. Shrotriya, J. Huang, Y. Yao, T. Moriarty, K. Emery and Y. Yang, *Nat. Mater.*, 2005, **4**, 864–868.
96 R. Kroon, M. Lenes, J. C. Hummelen, P. W. M. Blom and B. De Boer, *Polym. Rev.*, 2008, **48**, 531–582.
97 H. Y. Chen, J. H. Hou, S. Q. Zhang, Y. Y. Liang, G. W. Yang, Y. Yang, L. P. Yu, Y. Wu and G. Li, *Nat. Photonics*, 2009, **3**, 649–653.
98 V. I. Arkhipov, U. Wolf and H. Bässler, *Phys. Rev. B: Condens. Matter*, 1999, **59**, 7514.
99 H. Ma, H. L. Yip, F. Huang and A. K. Y. Jen, *Adv. Funct. Mater.*, 2010, **20**, 1371–1388.
100 R. Steim, F. R. Kogler and C. J. Brabec, *J. Mater. Chem.*, 2010, **20**, 2499–2512.
101 L. M. Chen, Z. Xu, Z. R. Hong and Y. Yang, *J. Mater. Chem.*, 2010, **20**, 2575–2598.
102 M. S. White, D. C. Olson, S. E. Shaheen, N. Kopidakis and D. S. Ginley, *Appl. Phys. Lett.*, 2006, **89**, 143517–143513.
103 F. S. Wen, W. L. Li, Z. Liu and H. Z. Wei, *Mater. Chem. Phys.*, 2006, **95**, 94–98.
104 A. W. Hains and T. J. Marks, *Appl. Phys. Lett.*, 2008, **92**, 023504.
105 M. D. Irwin, B. Buchholz, A. W. Hains, R. P. H. Chang and T. J. Marks, *Proc. Natl. Acad. Sci. U. S. A.*, 2008, **105**, 2783–2787.
106 V. Shrotriya, G. Li, Y. Yao, C.-W. Chu and Y. Yang, *Appl. Phys. Lett.*, 2006, **88**, 073508.
107 M. Kroger, S. Hamwi, J. Meyer, T. Riedl, W. Kowalsky and A. Kahn, *Org. Electron.*, 2009, **10**, 932–938.
108 M. Kroger, S. Hamwi, J. Meyer, T. Riedl, W. Kowalsky and A. Kahn, *Appl. Phys. Lett.*, 2009, **95**, 123301.
109 N. Li, B. E. Lassiter, R. R. Lunt, G. Wei and S. R. Forrest, *Appl. Phys. Lett.*, 2009, **94**, 023307–023303.
110 I. Hancox, K. V. Chauhan, P. Sullivan, R. A. Hatton, A. Moshar, C. P. A. Mulcahy and T. S. Jones, *Energy Environ. Sci.*, 2010, **3**, 107–110.
111 Irfan, H. J. Ding, Y. L. Gao, D. Y. Kim, J. Subbiah and F. So, *Appl. Phys. Lett.*, 2010, **96**, 073304.
112 J. Meyer, A. Shu, M. Kroger and A. Kahn, *Appl. Phys. Lett.*, 2010, **96**, 133308.
113 A. W. Hains, C. Ramanan, M. D. Irwin, J. Liu, M. R. Wasielewski and T. J. Marks, *ACS Appl. Mater. Interfaces*, 2010, **2**, 175–185.
114 A. W. Hains, J. Liu, A. B. F. Martinson, M. D. Irwin and T. J. Marks, *Adv. Funct. Mater.*, 2010, **20**, 595–606.
115 M. D. Irwin, J. Liu, B. J. Leever, J. D. Servaites, M. C. Hersam, M. F. Durstock and T. J. Marks, *Langmuir*, 2010, **26**, 2584–2591.

116 P. Peumans, V. Bulovic and S. R. Forrest, *Appl. Phys. Lett.*, 2000, **76**, 2650–2652.
117 D. Y. Kim, J. Subbiah, G. Sarasqueta, F. So, H. J. Ding, Irfan and Y. L. Gao, *Appl. Phys. Lett.*, 2009, **95**, 093304.
118 L. S. C. Pingree, B. A. MacLeod and D. S. Ginger, *J. Phys. Chem. C*, 2008, **112**, 7922–7927.
119 K. X. Steirer, J. P. Chesin, N. E. Widjonarko, J. J. Berry, A. Miedaner, D. S. Ginley and D. C. Olson, *Org. Electron.*, 2010, **11**, 1414–1418.
120 A. W. Hains and T. J. Marks, *Appl. Phys. Lett.*, 2008, **92**, 023504.
121 R. Betancur, M. Maymó, X. Elias, L. T. Vuong and J. Martorell, *Sol. Energy Mater. Sol. Cells*, 2011, **95**, 735–739.
122 S.-Y. Park, H.-R. Kim, Y.-J. Kang, D.-H. Kim and J.-W. Kang, *Sol. Energy Mater. Sol. Cells*, 2010, **94**, 2332–2336.
123 G. G. Malliaras and J. C. Scott, *J. Appl. Phys.*, 1999, **85**, 7426–7432.
124 M. A. Green, *Solid-State Electron.*, 1981, **24**, 788–789.
125 B. A. Gregg, S. G. Chen and R. A. Cormier, *Chem. Mater.*, 2004, **16**, 4586–4599.
126 B. A. Gregg, *MRS Bull.*, 2005, **30**, 20–22.
127 M. Glatthaar, N. Mingirulli, B. Zimmermann, T. Ziegler, R. Kern, M. Niggemann, A. Hinsch and A. Gombert, *Phys. Status Solidi A*, 2005, **202**, R125–R127.
128 D. Gupta, M. Bag and K. S. Narayan, *Appl. Phys. Lett.*, 2008, **93**, 163301.
129 K. H. Lee, P. E. Schwenn, A. R. G. Smith, H. Cavaye, P. E. Shaw, M. James, K. B. Krueger, I. R. Gentle, P. Meredith and P. L. Burn, *Adv. Mater.*, 2011, **23**, 766–770.

